MATCHING PERSISTENT SCATTERER CLUSTERS TO BUILDING ELEMENTS IN MESH REPRESENTATION

P. J. Schneider[1,*], U. Soergel[1]

[1] Institute for Photogrammetry (ifp), University of Stuttgart, Germany - (philipp.schneider, uwe.soergel)@ifp.uni-stuttgart.de

Commission III, WG III/3

KEY WORDS: Synthetic Aperture Radar, Persistent Scatterer Interferometry (PSI), Clustering, Data Fusion, Time Series Analysis, Building Information Modeling

ABSTRACT:

The deformation time series of Persistent Scatterer points show a correlated behavior if they lay on the same rigid structure and therefore undergo the same deformation process. By clustering, such groups of Persistent Scatterer (PS) points can be identified. We use segmented mesh representations of single buildings, to find the optimal assignment of such clusters to parts of the structure. By applying a quality metric, the assignment is judged quantitatively. The proposed method is useful for the integration of PSInSAR into building information modeling (BIM) and aims at a cost-effective city-wide per-building monitoring.

1. INTRODUCTION

Persistent scatterer interferometry (PSI) (Ferretti et al., 2000, 2001) developed over the last years to a widely used and well-excepted technique in the remote sensing community (Crosetto et al., 2016). This advanced differential interferometric synthetic aperture radar (DInSAR) evaluation technique can measure very small deformations in a wide area. This makes it interesting for city-wide monitoring applications. For high-resolution SAR data of urban scenarios the resulting PS-point clouds can be as dense as 1 PS per m^2 in particular on building facades (Schunert et al., 2012; Gernhardt et al., 2015). For each PS-point the movement in the line-of-sight direction can be estimated as a time series, in addition to the position.

The visualization and interpretation of such spatial-temporal data is challenging. In large-scale applications, such as volcano activity and earthquakes, velocity maps are a common way to present the estimated deformations. In single building monitoring, the observed motion processes are often caused by seasonal temperature change of annual periodic pattern (Crosetto et al., 2015). Schneider et al. (2020) have shown, that points that lay on the same rigid structure, and therefore are undergoing the same deformation process, show a correlated behavior in their time series. Schneider and Soergel (2021a,b) present a way to reliably find and cluster such correlated groups. This leads to the idea of linking those PS-clusters to parts of a building. To identify structural segments of a construction, a building information model (BIM) can be utilized. The optimal assignment between the PS-clusters and the structural elements, that are represented as a segmented mesh, is the main topic of this paper.

Related work has been carried out by Gernhardt et al. (2015) who investigated the origin and localization accuracy of PS-points on buildings by using detailed 3d models. Zhu et al. (2018) use a hierarchical clustering method to obtain groups of points that are more trustworthy. Costantini et al. (2018) follow a similar approach to detect the deformation anomalies that could cause building or infrastructure stability problems. The point-to-mesh association for geospatial data has been investigated by Laupheimer and Haala (2021) who suggest a face-centered geometry driven approach, to map airborne laser scanning data onto dense meshes e.g. for label transformation.

In contrast to the previously mentioned research, we use segmented meshes, that represent different parts of a structure, to map correlated PS-points onto. Such meshes can ideally be derived from BIM models or be manually created, based on high level of detail (LOD2+) models.

We choose two prominent buildings in Berlin, Germany, where High-Resolution Spotlight TerraSAR-X data are available as our study sites. Segmented meshes are created manually, based on publicly available unstructured models. A commercially Persistent Scatterer algorithm applied to extract PS-points on the building. We treat the PS time series and their positions as points in a high-dimensional space and use a custom distance metric and a non-linear dimension reduction technique to cluster them in a suitable fashion. For each of the mesh segments, the optimal cluster assignment is carried out. Finally, we present the meshes with the assigned clusters and their corresponding time series along with a quality criterion for the assignment.

In the following, we describe and explain the applied methods and the database, thereby we focus on the mesh segmentation and the optimal assignment between clusters and segments. Briefly discussed are also the disadvantages of a linear model in PS motion estimation, especially for applications on large steel structures. The final results are complemented by a link to a web platform that allows the three-dimensional data to be viewed from all sides.

2. METHODS AND DATABASE

2.1 Study Site

As exemplary study sites, we choose buildings in our scene based on two criteria: firstly the building must be large enough

*Corresponding author

https://doi.org/10.5194/isprs-annals-V-3-2022-123-2022 | © Author(s) 2022. CC BY 4.0 License.

so a significant amount of persistent scatterers can be found, secondly a detailed mesh model must be available.

As the main study site, we choose the *Reichstag Building*. This neo-renaissance building underwent reconstruction in the 1990s. The building can be roughly divided into its four wings and the characteristic glass-steel cupola in the center (Figure 3).

As a second building, we choose the *Berlin Central Station*. This structure is especially interesting because many previous DInSAR publications have used it as an example (Gernhardt and Bamler, 2015; Gernhardt et al., 2010a; Wang and Zhu, 2015; Montazeri et al., 2015). The terminal consists of a long pier bridge on which the tracks run, and two large main buildings perpendicular to it. The bigger part of the platform is covered by a glass roof (Figure 8/9).

2.2 SAR-Data and PSI

The synthetic aperture radar (SAR) data for our experiments is a stack of TerraSAR-X images in High-Resolution Spotlight mode (Airbus, 2017), acquired during a 3 year time span over Berlin, Germany (Tab. 1). Relative to the master image, the spatial baselines do not exceed 250 m (Figure 1).

Based on the original idea of Persistent Scatterer Interferometry (PSI) (Ferretti et al., 2001, 2000), several comercial software solutions are available.

We processed the SAR data with the PS-module in SARscape 5.5 (SARMAP, 2014), the software is designed to estimate displacements characterized by a linear trend $\mathrm{Def}(t) = v \cdot t$. This assumption can have a negative impact on the deformation estimates of all phenomena characterized by non-linear deformation behavior, where the assumption is not valid. The PSI products based on the linear assumption typically lack PSs in all areas where the deformation shows significantly non-linear motion, because there is a misfit between the linear model and the observed (non-linear) deformation (Crosetto et al., 2015, 2016).

The result from the PS-analysis is an estimated 3d coordinate for each PS-point along with a time series $\mathrm{Def}(t)$ that depicts the line-of-sight (LOS) movement of this point towards the satellite. While the 3d accuracy of the coordinate is usually in the order of meters, the deformation time series for X-band SAR can be in the mm/year scale, provided that the above-mentioned deformation model represents the underlying displacement processes (Gernhardt et al., 2015; Quin and Loreaux, 2013).

We observe this lack of PS-points on the railway station with a (temporal model) coherence, value > 0.6 (Figure 10). This is consistent with findings by Gernhardt (2011) (p. 150ff) who estimates a seasonal component of those parts with an amplitude $> 10\,\mathrm{mm}$, using a non-linear deformation model. Since we are not interested in the actual movement, but in the correlated behavior of PS-points on the building, we include points down to the low coherence threshold of 0.4 to receive points on the highly non-linear moving parts of the building. These results have to be interpreted very carefully since the estimated linear trends in Figure 10 do not represent the actual underlying deformation processes and have to be considered as a processing artifact, due to the linear model.

For the second building, we do not observe those strong annual oscillations. The underlying deformation model is sufficient and a temporal model coherence threshold of 0.6 leads to a dense distribution of PS-points on all parts the building (Figure 2 & 3).

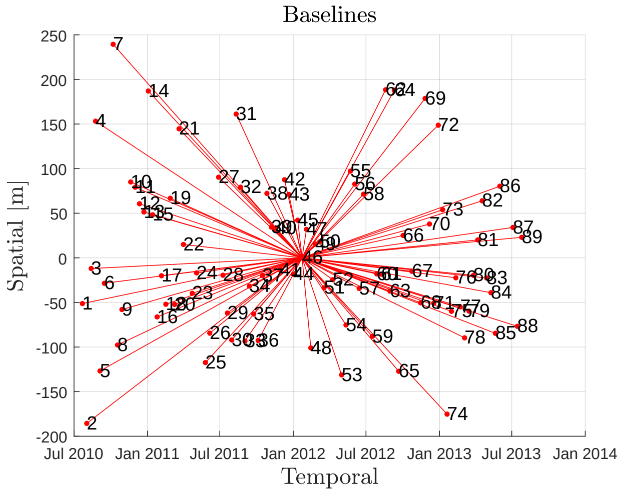

Figure 1. Temporal and spatial baselines, relative to the master image from 23rd January 2012. The 89 images were acquired between 22nd July 2010 and 26th July 2013, with a repeat interval of 11 days.

Platform	TerraSAR-X
Wavelength	31mm (9.6 GHz, X-Band)
Acquisition Mode	HS, Spot 042, VV, R
Central Point	N52° 31'30.5" E13° 22' 3.9"
Orbit Direction	Descending
Resolution: Ra × Az	0.6 m × 1.1 m
Number of Images	89
Time interval	22.07.2010 - 26.07.2013
Repeat Time	11 Days
PS-Algorithm	L3 SARscape 5.5
Date of Master	23.01.2012
Processing Coherence	0.3

Table 1. SAR Data acquisition and processing parameters.

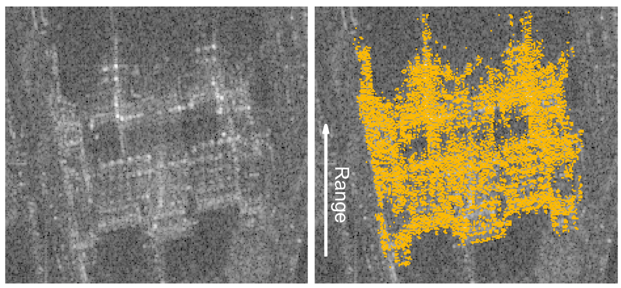

Figure 2. The *Reichstag* in SLC Image with PS-points (right). The SAR-typical imaging geometry: layover, foreshortening and shadowing lead to a highly distorted image of building. During the PS-processing, the actual spatial distribution for all PS-points is estimated.

2.3 Segmented Mesh

A building's physical extension can be modeled as a polyhedral object. Polygon meshes are widely used in computer graphics to describe such objects. Meshes generally consist of vertices

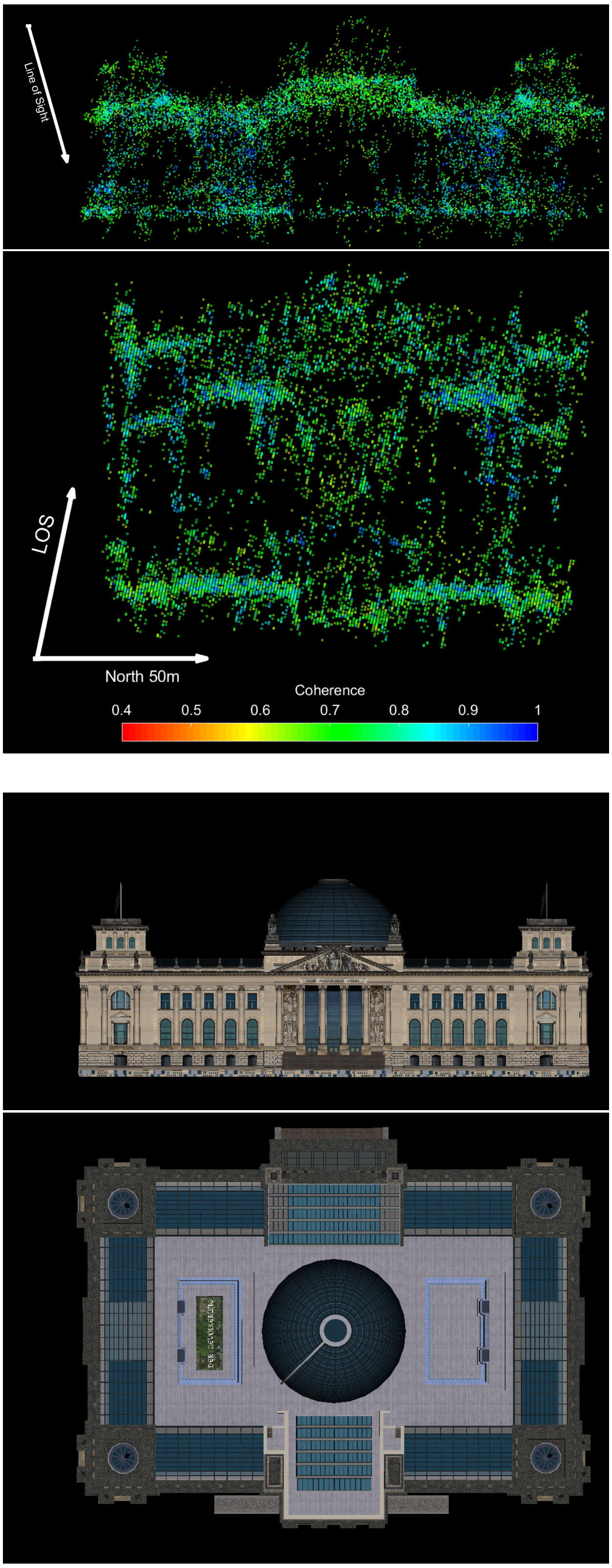

Figure 3. Top: PS-points with color coded coherence from side and top view. Bottom: Textured mesh of the same building (side and top view). Note that the PS-point density on the facades, towards the line-of-sight is is very dense. Also the steel structures on the roof lead to a high point density, with a high coherence value.

and faces. Vertices are defined by points in 3d space. Faces are described by at least 3 combined vertices. Additional more per-face and/or per-vertex attributes, like material, color, or texture, can be defined. For geospatial data, meshes have several applications, e.g., a lean representation of densely textured city models or the appearance of buildings in LOD1-LOD4 and building information models (BIM). In BIM those 3D geometries represent the physical and functional characteristics of a facility. Depending on the use case of the BIM, parts like walls, beams, pipes, segments, windows, etc. are modeled. This adds a second layer to the before unstructured mesh: semantic. Such a structured segmented mesh represents individual parts of a building. A model of this kind can be used to monitor a structure over its lifespan, by assigning measurements to parts and analyses of their interactions. Nowadays the existence of such ”as build” BIM data is still rare but in the near future BIM-based design, construction and maintenance will be the standard for complex projects (Isikdag, 2015).

Since we could not get a hold on a ”as build” model we used a freely available high detailed model of the *Reichstag* by AleXBY (2015) and segmented it into substructures, in a best effort manner, as shown in Figure 4. For the *Berlin Central Station* we used an unstructured mesh from Arndt (2021) and manually created a segmented building model for our analysis. The segmentation is based on visible major structural elements like bridge piers, expansion joints, steel girders, and floors. In Figure 9 each segment is shown in a different color.

It is known that both buildings do not suffer from linear deformation process, hence we assume that any observed motion is due to thermal expansion. In the following process, we treat these segments as individual parts of the building. Each part is subject to thermal expansion and contraction processes with an annual period. The assumption is that PS-points on those structures show a highly correlated deformation history and can therefore be clustered into groups, which can be assigned to the individual parts. The result of this assignment directly depends on the quality of the segmentation. If the manually constrained segments do not represent the actual structure or are too coarse, the correspondence is estimated falsely.

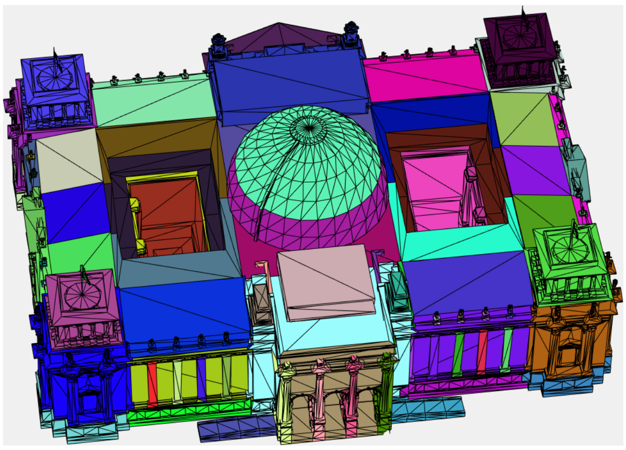

Figure 4. Manualy segmented mesh of the *Berlin Reichstag* - each color indicates an individual segment

2.4 PS- Point clustering

We treat the deformation history $\mathrm{Def}(t)$ of each PS-point as a point in a 89-dimensional space, with a dimension for each acquisition date. Each point $d_n \in \mathbb{R}^M$ is defined by the $M = 89$

https://doi.org/10.5194/isprs-annals-V-3-2022-123-2022 | © Author(s) 2022. CC BY 4.0 License.

measurements:

$$d_n = \begin{bmatrix} d_1^n & d_2^n & \dots & d_{M-1}^n & d_M^n \end{bmatrix}. \tag{1}$$

The assumption is that points that lay on a rigid structure show similar deformation behavior and therefore form clusters in deformation space. Clustering directly in this high-dimensional space goes along with the various curse of dimensionality problems (Allaoui et al., 2020).

Instead, we use a non-linear dimension reduction method with a hybrid distance metric followed by a clustering process to extract such clusters from the PS-point cloud, as proposed by Schneider and Soergel (2021b). That means, we embed the points $d_n \in \mathbb{R}^M$ into a low dimensional space $d'_n \in \mathbb{R}^2$ while preserving local neighborhoods, using UMAP (McInnes et al., 2018). The distance D of two points is defined by a combination of the Pearson correlation D_C and the Euclidean distance D_E as described by Schneider and Soergel (2021a):

$$D = \sqrt{D_C^2 + D_E^2}\,. \tag{2}$$

After a noise floor estimation by analyzing the Core Distance Graph (Ankerst et al., 1999), DBSCAN (Ester et al., 1996) is used to extract clusters. The embedding with the extracted clusters is shown in Figure 6.

Each of the clusters represents a group of PS-points that move in a correlated way and are not too far apart on the building. For each of the clusters, the centroid can be analyzed. If treated as a time series one can derive the mean deformation history for each cluster. In Figure 7 the centroids for the extracted clusters from *Reichstag* are shown.

2.5 Cluster to Segment Assignment

Our cluster to segment assignment workflow aims to treat the task as a one (cluster) to many (segments) assignment problem. The goal is to assign each of the J segments to one of the I clusters. That means that one cluster can be assigned to multiple parts of a building.

To find the optimal assignment, we use a variant of the Hungarian algorithm (Kuhn, 1955). Generally spoken, this algorithm finds the optimal one-to-one assignment for a given bipartite graph, that is described by a qualification matrix Q.

For the qualification matrix Q, we use „1-the normalized vertex neighbor count“ $1 - ||C||$ for each segment. For each vertex in the mesh, we count the class (cluster) appearance in the $k = 10$ closest PS-points. For each segment, this count is normalized by the total count.

To achieve a one-to-many assignment, we concatenate the qualification matrix Q several times.

A short example for $I = 3$ clusters and $J = 5$ segment is given in the following:

The vertices in $Segment_1$ have 50 k-closest neighbors to $Cluster_1$, 20 k-closest neighbors to $Cluster_2$ and no neighboring PS-points to $Cluster_3$ etc. this leads to the connection Matrix C:

$$C = \left(\begin{array}{c|ccccc} & Seg_1 & Seg_2 & Seg_3 & Seg_4 & Seg_5 \\ \hline Cl_1 & 50 & 0 & 30 & 60 & 0 \\ Cl_2 & 20 & 20 & 10 & 30 & 0 \\ Cl_3 & 0 & 10 & 10 & 40 & 60 \end{array}\right) \tag{3}$$

By normalizing the columns of C, by dividing them through the sum, we can compensate for parts with higher vertex counts in the normalized cost matrix connection matrix $||C||$:

$$||C|| = \left(\begin{array}{c|ccccc} & Seg_1 & Seg_2 & Seg_3 & Seg_4 & Seg_5 \\ \hline Cl_1 & 0.71 & 0.0 & 0.60 & 0.46 & 0.00 \\ Cl_2 & 0.29 & 0.67 & 0.20 & 0.23 & 0.00 \\ Cl_3 & 0.0 & 0.33 & 0.20 & 0.31 & 1.00 \end{array}\right) \tag{4}$$

If we would use $1 - ||C||$ as the qualification matrix in the Hungarian algorithm, we would not be able to assign one cluster to multiple segments. We overcome this limitation by concatenating the $||C||$ vertically for multiple times (two times in this example):

$$Q = 1 - \begin{bmatrix} ||C|| \\ ||C|| \end{bmatrix} \tag{5}$$

$$= 1 - \left(\begin{array}{c|ccccc} & Seg_1 & Seg_2 & Seg_3 & Seg_4 & Seg_5 \\ \hline Cl_1 & 0.71 & 0.0 & 0.60 & 0.46 & 0.00 \\ Cl_2 & 0.29 & 0.67 & 0.20 & 0.23 & 0.00 \\ Cl_3 & 0.0 & 0.33 & 0.20 & 0.31 & 1.00 \\ Cl'_1 & 0.71 & 0.0 & 0.60 & 0.46 & 0.00 \\ Cl'_2 & 0.29 & 0.67 & 0.20 & 0.23 & 0.00 \\ Cl'_3 & 0.0 & 0.33 & 0.20 & 0.31 & 1.00 \end{array}\right) \tag{6}$$

The optimal assignment for this example would be:

$$\begin{array}{c|ccccc} & Seg_1 & Seg_2 & Seg_3 & Seg_4 & Seg_5 \\ \hline Cl_1 & 1 & 0 & 1 & 0 & 0 \\ Cl_2 & 0 & 1 & 0 & 0 & 0 \\ Cl_3 & 0 & 0 & 0 & 1 & 1 \end{array} \tag{7}$$

Note how the number of concatenations allows multiple assignments of each cluster to different segments. In our experiments, we set this to 10.

2.6 Quality Metric

The quality of the assignment mainly depends on how well the mesh segments represent the borders of the clusters. If multiple clusters fall on one segment, the corresponding column in $||C||$ (4) would have a wide distribution. Such a histogram of class affiliation can be described by entropy. We calculate a per segment-entropy from $||C||$ as follows:

$$H(Seg_j) = \sum_{i=1}^{I} ||C_{i,j}|| \cdot log_2(||C_{i,j}||) \tag{8}$$

high entropy values indicate poor cluster-segment allocation, whereby low values indicate a good match.

3. RESULTS

We find sufficient PS-point for the *Reichstag* building (Figure 2). The embedding in the 2d dimensional space, followed by the cluster extraction shows plausible groups of PS-points (Figure 6 a)). The time series for most clusters can be interpreted as small annual temperature-induced seasonal oscillations with an amplitude $< 5\,\mathrm{mm}$ in the line-of-sight direction (Figure 7). The matching of these extracted clusters to segments of the mesh works especially well for the four turrets and the upper part of the cupola. The per-segment entropy in Figure 6 b) suggests that the manually divided mesh is not definite for some parts. This is coherent with a visual inspection of the parts and the clusters.

We also present the results for the second test site *Berlin Central Station* in the Appendix. Figure 8 shows the PS-points in the SLC scene, next to an orthophoto. As mentioned in 2.2, the PSI software we use is not capable of reliably extracting PS-points that underlay a highly non-linear deformation process. Figure 10 shows that in areas of low temporal model coherence, the estimated linear velocity is high. Nevertheless, our approach also works with falsely estimated time series. We can successfully extract plausible clusters from the PS-points and link them to the manually segmented mesh (Figure 11). Noteworthy, the clusters coincide with the bridge piers and expansion joints presented by Gernhardt et al. (2010b), which affects the per-segment entropy in those areas to be good.

For the better interpretation, we also provide a website with a 3d visualization of these results. The three-dimensional nature of these data makes it much easier to understand, if viewed from different perspectives (Figure 5).

`https://ifpwww.ifp.uni-stuttgart.de/philipp/ISPRS2022/rst/`

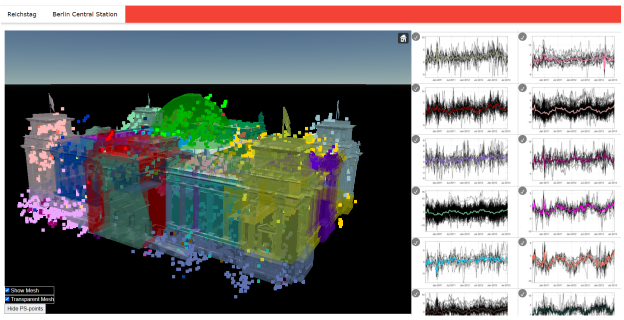

Figure 5. A web portal with the presented results. Left: Mesh superimposed with the PS-points. The clusters are color coded and correspond with the extracted time series on the right hand side. The user can move the mouse over a time series to highlight it in the 3d view, freely rotate and zoom and show/hide the mesh and the points.

4. CONCLUSION AND OUTLOOK

We presented an approach to link PSInSAR data with mesh representations of a building. While the extraction of Persistent Scatterer (PS) points has its own challenges, especially with non-linear deformations, the interpretation and presentation of a huge number of PS-points have been investigated here. The overall goal of this work is the integration of continuous, city-wide InSAR measurements into a single building monitoring. This would highly profit from the availability of building information modeling (BIM) data, where each structural element is represented by an individual instance. The lack of suitable as-built BIM models led us to generate our own segmented meshes from freely available city models. The experiments on the two test sites showed that the extracted PS-clusters can automatically and plausible be combined with the segmented mesh, using an optimal assignment algorithm.

For the future and current work, we are trying to get our hands on actual as-built models in areas where high-resolution SAR data is available. We are optimistic that both are broadly available in the future.

Since we could not satisfactorily extract PS-points on the building parts that undergo a periodical movement, a non-linear Persistent Scatterer Interferometry approach is very important for building monitoring. Interesting work is carried out by Ogushi et al. (2019, 2021) and we hope that this will lead to wider availability of this powerful remote-sensing technique in the future.

ACKNOWLEDGEMENTS

This research was partially founded by by the German Federal Ministry for Economic Affairs and Climate Action. We want to thank the Federal Republic of Germany's research centre for aeronautics and space (DLR) for providing us the necessary TerraSAR-X images. Furthermore want to acknowledge the open data policy of the Berlin's Senate Department for Urban Development and Housing, Department III - Geoinformation, their uncomplicated and practical approach to public data provided us a digital surface model and the mesh of the central station. Last but not least we want to appreciate the work of the unknown user AleX_BY, who created and provides the detailed model of the Reichstag.

Revised March 2022

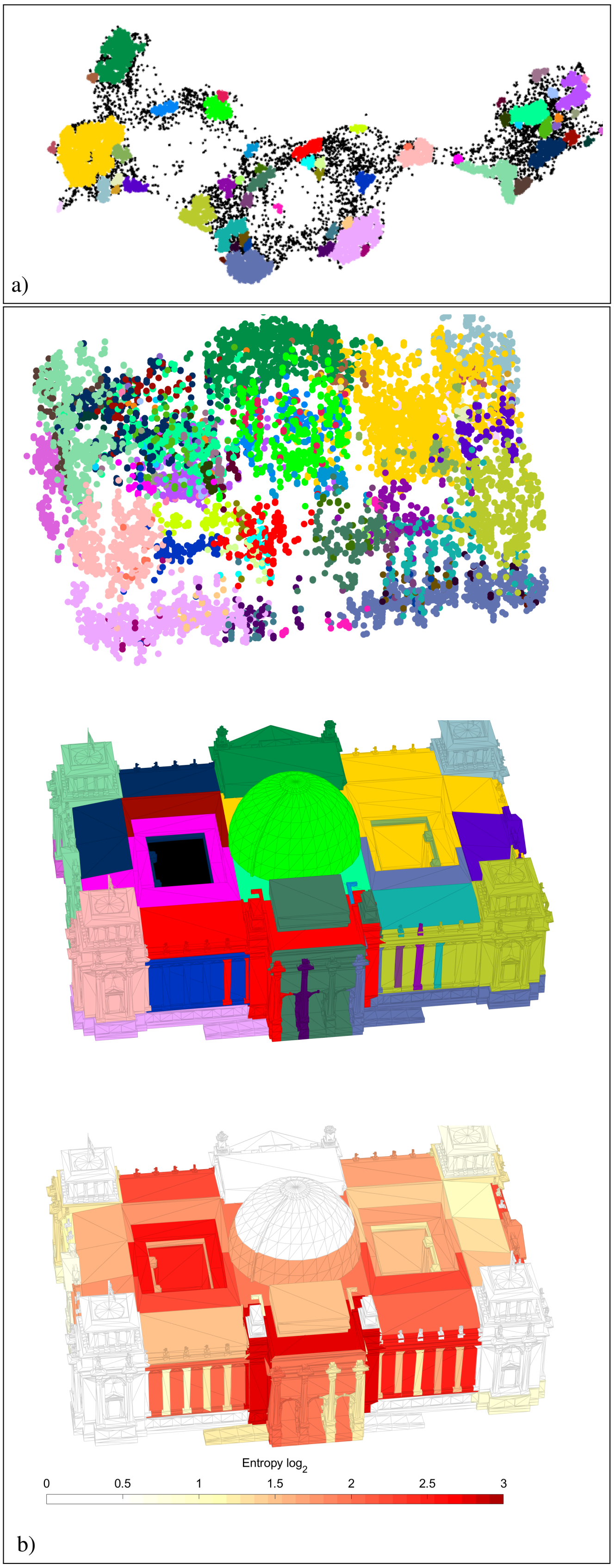

Figure 6. **a)** Embedding of the PS-points in 2d deformations space. The extracted clusters are shown in different colors. **b)** Top: PS-point on *Reichstag* all the colors correspond to a) and Figure 7. Middle: Mesh colored with the assigned PS-cluster. Bottom: Entropy for each mesh segment. A lower entropy indicates a good match between the cluster and the segment.

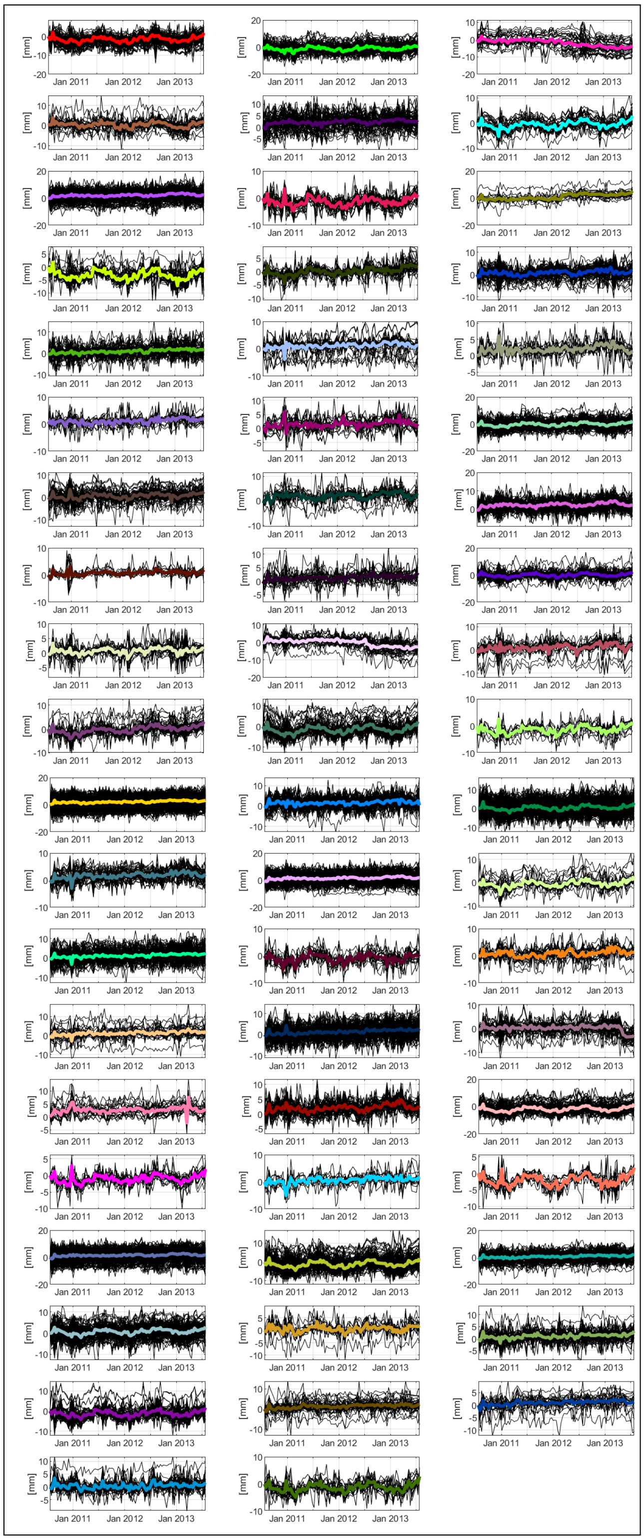

Figure 7. Time series for the extracted PS-clusters. The colored line indicates the mean deformation for the cluster. The colors correspond to Figure 6.

APPENDIX

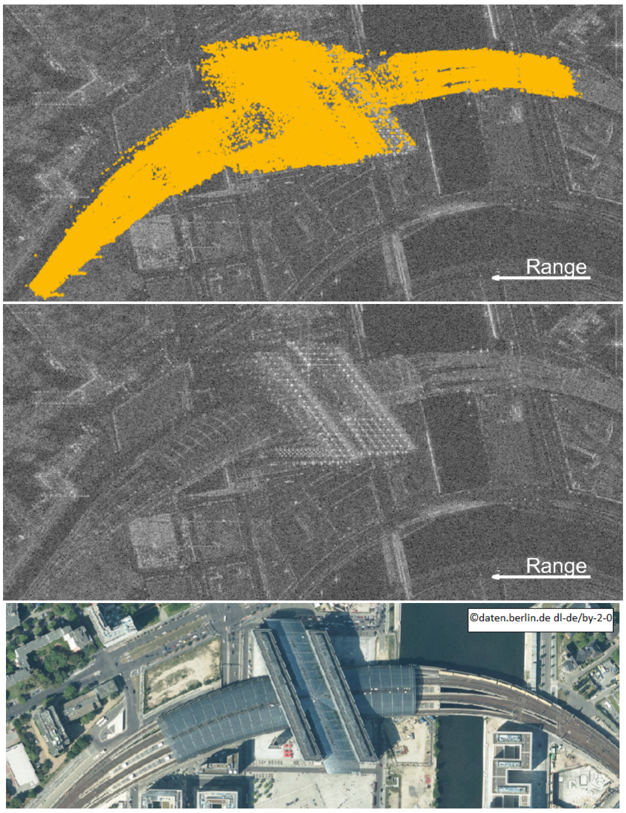

Figure 8. Top/Middle: SLC Image with and without PS-points on *Berlin Central Station*. Bottom: Orthophoto of the same scene.

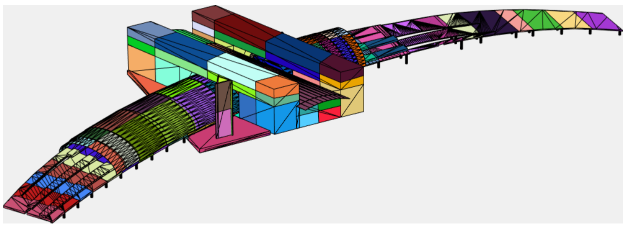

Figure 9. Manually segmented mesh of the *Berlin Central Station* - each color indicates an individual segment

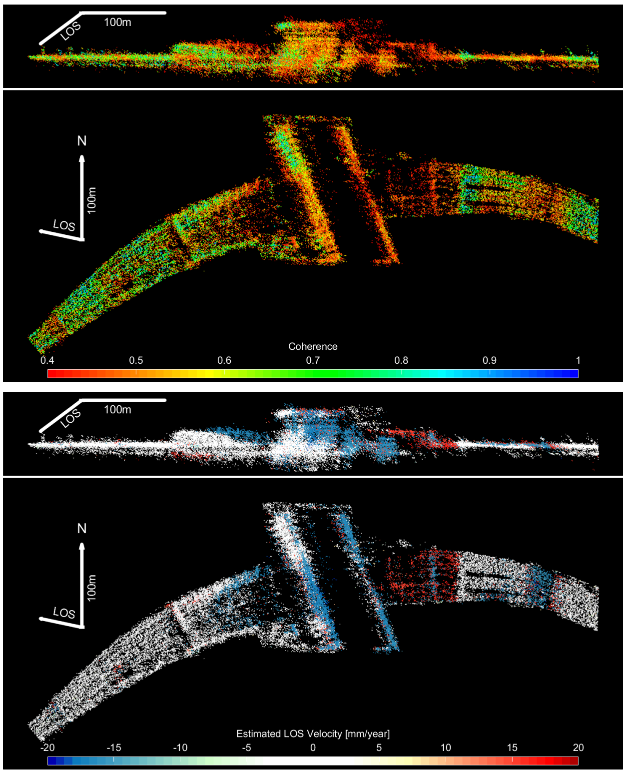

Figure 10. PS-points on *Berlin Central Station* from side and top view. Top: with color coded temporal model coherence. Bottom: with estimated linear velocities (linear model).

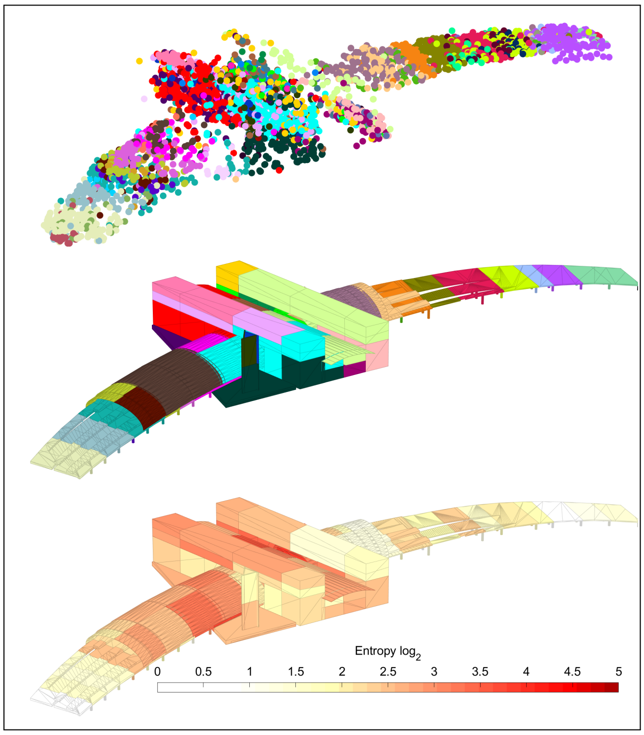

Figure 11. Top: PS-point on *Berlin Central Station*. Each extracted cluster in a different color. Middle: Mesh colored with the assigned PS-cluster. Bottom: Entropy for each mesh segment. A lower entropy indicates a good match between the cluster and the segment.

REFERENCES

Airbus, 2017. TerraSAR-X Image Product Guide - Basic and Enhanced Radar Satellite Imagery. (February 2020). `https://www.intelligence-airbusds.com/files/pmedia/public/r459_9_20171004_tsxx-airbusds-ma-0009_tsx-productguide_i2.01.pdf`.

Allaoui, M., Kherfi, M. L. and Cheriet, A., 2020. Considerably improving clustering algorithms using umap dimensionality reduction technique: A comparative study. In: A. El Moataz, D. Mammass, A. Mansouri and F. Nouboud (eds), *Image and Signal Processing*, Springer International Publishing, Cham, pp. 317–325.

Ankerst, M., Breunig, M. M., Kriegel, H.-P. and Sander, J., 1999. OPTICS. *ACM SIGMOD Record* 28(2), pp. 49–60.

Arndt, W., 2021. 3D-Modell Digitale Innenstadt. Senatsverwaltung für Stadtentwicklung und Wohnen.

Costantini, M., Zhu, M., Huang, S., Bai, S., Cui, J., Minati, F., Vecchioli, F., Jin, D. and Hu, Q., 2018. Automatic detection of building and infrastructure instabilities by spatial and temporal analysis of insar measurements. *IGARSS 2018 - 2018 IEEE International Geoscience and Remote Sensing Symposium* pp. 2224–2227.

Crosetto, M., Monserrat, O., Cuevas-González, M., Devanthéry, N. and Crippa, B., 2016. Persistent scatterer interferometry: A review. *ISPRS Journal of Photogrammetry and Remote Sensing* 115, pp. 78–89.

Crosetto, M., Monserrat, O., Cuevas-González, M., Devanthéry, N., Luzi, G. and Crippa, B., 2015. Measuring thermal expansion using X-band Persistent Scatterer Interferometry. *ISPRS Journal of Photogrammetry and Remote Sensing* 100, pp. 84–91.

Ester, M., Kriegel, H.-P., Sander, J. and Xu, X., 1996. A density-based algorithm for discovering clusters in large spatial databases with noise. In: *Proceedings of the Second International Conference on Knowledge Discovery and Data Mining*, KDD'96, AAAI Press, pp. 226–231.

Ferretti, A., Prati, C. and Rocca, F., 2000. Nonlinear subsidence rate estimation using permanent scatterers in differential sar interferometry. *Geoscience and Remote Sensing, IEEE Transactions on* 38, pp. 2202 – 2212.

Ferretti, A., Prati, C. and Rocca, F., 2001. Permanent scatterers in SAR interferometry. *IEEE Transactions on Geoscience and Remote Sensing* 39(1), pp. 8–20.

Gernhardt, S., 2011. High precision 3D localization and motion analysis of persistent scatterers using meter-resolution radar satellite data. PhD thesis, Technische Universität München.

Gernhardt, S., Adam, N., Eineder, M. and Bamler, R., 2010a. Potential of very high resolution sar for persistent scatterer interferometry in urban areas. *Annals of GIS* 16, pp. 103–111.

Gernhardt, S., Adam, N., Eineder, M. and Bamler, R., 2010b. Potential of very high resolution SAR for persistent scatterer interferometry in urban areas. *Annals of GIS* 16(2), pp. 103–111.

Gernhardt, S. and Bamler, R., 2015. Structural deformation and non-seasonal motion of single buildings in urban areas revealed by PSI. In: *2015 Joint Urban Remote Sensing Event (JURSE)*, IEEE.

Gernhardt, S., Auer, S. and Eder, K., 2015. Persistent scatterers at building facades – evaluation of appearance and localization accuracy. *ISPRS Journal of Photogrammetry and Remote Sensing* 100, pp. 92–105.

Isikdag, U., 2015. The future of building information modelling: BIM 2.0. In: *Enhanced Building Information Models*, Springer International Publishing, pp. 13–24.

Kuhn, H. W., 1955. The hungarian method for the assignment problem. *Naval Research Logistics Quarterly* 2(1-2), pp. 83–97.

Laupheimer, D. and Haala, N., 2021. Juggling with representations: On the information transfer between imagery, point clouds, and meshes for multi-modal semantics. *ISPRS Journal of Photogrammetry and Remote Sensing* 176, pp. 55–68.

McInnes, L., Healy, J., Saul, N. and Großberger, L., 2018. Umap: Uniform manifold approximation and projection. *Journal of Open Source Software* 3(29), pp. 861.

Montazeri, S., Zhu, X. X., Eineder, M., Hanssen, R. and Bamler, R., 2015. Deformation monitoring of urban infrastructure by tomographic SAR using multi-view TerraSAR-x data stacks. In: *Proceedings of Fringe 2015: Advances in the Science and Applications of SAR Interferometry and Sentinel-1 InSAR Workshop*, European Space Agency.

Ogushi, F., Matsuoka, M., Defilippi, M. and Pasquali, P., 2021. Implementation of non-linear non-parametric persistent scatterer interferometry and its robustness for displacement monitoring. 21(3), pp. 1004.

Ogushi, Matsuoka, Defilippi and Pasquali, 2019. Improvement of persistent scatterer interferometry to detect large non-linear displacements with the 2π ambiguity by a non-parametric approach. 11(21), pp. 2467.

Quin, G. and Loreaux, P., 2013. Submillimeter accuracy of multipass corner reflector monitoring by PS technique. *IEEE Transactions on Geoscience and Remote Sensing* 51(3), pp. 1775–1783.

SARMAP, 2014. Sarscape: Ps tutorial. `https://www.sarmap.ch/tutorials/PS_Tutorial_V_0_9.pdf`.

Schneider, P. J. and Soergel, U., 2021a. Clustering persistent scatterer points based on a hybrid distance metric. In: *Lecture Notes in Computer Science*, Springer International Publishing, pp. 621–632.

Schneider, P. J. and Soergel, U., 2021b. Segmentation of buildings based on high resolution persistent scatterer point clouds. *ISPRS Annals of the Photogrammetry, Remote Sensing and Spatial Information Sciences* V-3-2021, pp. 65–71.

Schneider, P. J., Khamis, R. and Soergel, U., 2020. Extracting and evaluating clusters in DInSAR Deformation data on single buildings. *ISPRS Annals of Photogrammetry, Remote Sensing and Spatial Information Sciences* V-3-2020, pp. 157–163.

Schunert, A., Schack, L. and Soergel, U., 2012. Matching Persistent Scatterers to Buildings. *ISPRS - International Archives of the Photogrammetry, Remote Sensing and Spatial Information Sciences* XXXIX-B7, pp. 79–84.

AleXBY, 2015. "Reichstag building [+AD]" Accessed November 2021. `https://steamcommunity.com/sharedfiles/filedetails/?id=421085355`.

Wang, Y. and Zhu, X. X., 2015. Automatic feature-based geometric fusion of multiview TomoSAR point clouds in urban area. *IEEE Journal of Selected Topics in Applied Earth Observations and Remote Sensing* 8(3), pp. 953–965.

Zhu, M., Wan, X., Fei, B., Qiao, Z., Ge, C., Minati, F., Vecchioli, F., Li, J. and Costantini, M., 2018. Detection of building and infrastructure instabilities by automatic spatiotemporal analysis of satellite sar interferometry measurements. *Remote Sensing* 10(11), pp. 1816.